

# Light scattering from red pigment particles: Multiple scattering in a strongly absorbing system

L. E. McNeil<sup>a)</sup>

*Department of Physics and Astronomy, University of North Carolina at Chapel Hill, Chapel Hill, North Carolina 27599-3255*

R. H. French

*DuPont Central Research and Development, Wilmington, Delaware 19880-0356*

(Received 15 May 2000; accepted for publication 16 October 2000)

In the optical analysis of collections of particles embedded in a matrix, the ultimate goal is to predict the optical properties of the final film, given the optical characteristics of the materials of which it is made, the particle size, and the fraction of the volume occupied by the particles. The first task in the pursuit of this goal is to make connections between the optical properties of the bulk materials of which the particles and medium are made and the spatial distribution of the scattered intensity from the individual particles. The second is to relate the calculated far-field scattering and absorption cross sections for a single particle to the measured optical characteristics of real films. Here we accomplish these tasks for a regime that is rarely considered in the literature but is quite important in applications. This regime is characterized by three conditions: (a) the extinction coefficient of the particle is significant; (b) the particle size is comparable to the wavelength in the medium; and (c) the optical density of the films is large enough that multiple scattering is significant, and yet direct transmission of collimated radiation through the film is not negligible. We have measured the visible diffuse reflectance and transmission of films of quinacridone particles in a transparent resin at various particle volume concentrations, and used the Kubelka–Munk formalism as a parametrization method to extract scattering and absorption parameters for this strongly absorbing, multiple-scattering system in the resonant regime. We have modeled the scattering parameter  $S^*$  as a convolution of the angular distribution of the scattering from a single particle (derived from Mie theory) and a multiple-scattering function that characterizes the effects of the concentration and arrangement of the particles in the film. We find that the multiple-scattering function has an angular distribution that is strongly peaked in the backscattering direction. This accounts for the transformation of the collimated and strongly forward-scattered light in the top layers of the film into diffusely reflected light as the film is traversed. The multiple-scattering function also accounts for the differences in diffuse reflection observed for films of identical volume fraction occupied by particles (particle volume concentration) but different grinding time. This method of analysis begins to allow one to make an explicit connection between the fundamental optical properties of the particles and the experimentally accessible parameters. We have thus developed a way to begin to bridge the gap between the fundamental physics of the scattering of light from individual particles and the practical characterization of a film using the simple Kubelka–Munk analysis. © 2001 American Institute of Physics. [DOI: 10.1063/1.1331344]

## I. INTRODUCTION

The subject of the scattering of electromagnetic radiation by particles is an old and wide-ranging one. Its applications include such phenomena as the blue sky and other atmospheric phenomena,<sup>1</sup> the obscuration of galaxies by interstellar dust,<sup>2</sup> the curing of photopolymers for stereolithography,<sup>3</sup> the transparency of fishes<sup>4</sup> and the human cornea,<sup>5</sup> and the appearance of reflective display materials,<sup>6</sup> paint,<sup>7</sup> and paper.<sup>8</sup>

For single particles of simple shapes, it is possible to calculate analytically the intensity of the scattered light in the far field. If the particles are sufficiently far apart that the

scattered radiation from the different particles is simply additive, then the scattering can be completely described by this analysis. If the particle density is sufficiently high, or the optical depth is sufficiently large, then it is necessary to account for multiple scattering as the light scattered by one particle impinges upon another. Various models have been developed to treat multiple scattering, typically in the case where the particles are not strongly absorbing and are small compared to the wavelength of the light. Other models, such as that of Kubelka and Munk,<sup>9</sup> treat the scattering as if it arose from a continuous medium rather than a collection of particles. The mathematical simplicity of such a treatment is offset by the loss of an explicit connection with the optical properties of the individual particles that make up the medium.

<sup>a)</sup> Author to whom all correspondence should be addressed; electronic mail: mcnail@physics.unc.edu

In this paper we address a regime that is rarely considered in the literature but is quite important in applications. This regime is characterized by three conditions: (a) the extinction coefficient of the particle is significant; (b) the particle size is comparable to the wavelength in the medium; and (c) the optical density of the films is large enough that multiple scattering is significant, and yet direct transmission of collimated radiation through the film is not negligible. In the single-scattering regime, the first two conditions do not present significant difficulties, particularly if the particles are approximately spherical. Some methods have been developed for dealing with condition (c), such as the many-flux picture of Meheu,<sup>10</sup> and the photon diffusion model of Gate<sup>11</sup> as well as numerical studies based on Monte Carlo simulations. However, each of these models, as worked out in the literature, involves assumptions that are often not appropriate for realistic situations. Although systems satisfying each of these conditions have been treated in the literature, there appears to have been no discussion of the complicated (but realistic) situation when all of the conditions apply.

The specific example of this regime that we consider here is the case of films made up of quinacridone pigment particles in a transparent resin, analyzed in the visible light range. The pigment and resin are typical of those used in coatings to protect and color the exterior of an automobile body (i.e., paints). Quinacridone has two strong absorption bands in the near-UV and green portions of the spectrum, which color the films red in reflection and transmission. The fraction of the total volume occupied by the pigment particles in the films considered here is also typical of those used in the manufacture of automotive coatings. The three conditions listed previously are fulfilled as follows. (a) The particle extinction coefficient  $k_{\text{particle}}$  is in the range  $10^{-2} < k_{\text{particle}} < 1$  for all but the longest wavelengths in the range. (b) The size parameter  $x = 2\pi a n_{\text{medium}}/\lambda$ , where  $a$  is the diameter of the particle,  $\lambda$  is the wavelength of light in vacuum, and  $n_{\text{medium}}$  is the index of refraction of the resin at  $\lambda$ , is in the range  $5 < x < 20$ . (c) The optical density  $\tau = (\eta + \chi)d$ , where  $\eta$  and  $\chi$  are the single-particle scattering and absorption cross sections multiplied by the number density of the particles, and  $d$  is the film thickness, is in the range  $4 < \tau < 27$ . However, a non-negligible portion of the collimated incident light is directly transmitted, so that the ratio of the diffuse to the total transmittance  $T_{\text{diffuse}}/T_{\text{total}}$  is in the range  $0.4 < T_{\text{diffuse}}/T_{\text{total}} < 1$ .

Our ultimate goal in this project is to be able to predict the optical properties of the final film, given the optical characteristics of the materials of which it is made, the particle size, and the fraction of the volume occupied by the particles. This prediction could take the form of calculated diffuse reflectance and transmittance spectra, or of calculations of easily measured quantities such as the Kubelka–Munk parameters. The first form is of more fundamental interest, while the second is often of more immediate use to practitioners of the art of paint formulation.

In our pursuit of this ultimate goal, we have identified several near-term goals to be achieved along the way. The first is to explicitly examine the far-field scattering from a single particle in resin, in order to provide a basis for under-

standing the influence of the optical constants of the materials on the scattering. We seek to make connections between the optical properties of the bulk materials of which the particles and resin are made and the spatial distribution of the scattered intensity from the individual particles. This goal is achieved with the use of Mie theory. We have applied this well-known analytic method to obtain insights about a particular system of considerable technological importance.

Our second near-term goal is to relate the calculated far-field scattering and absorption cross sections for a single particle to the measured optical characteristics of real films. This is achieved by modeling the angular distributions of the scattered light that result from single and multiple scattering, and comparing the results to the measured diffuse reflectance and transmittance. We then identify how the models transform as parameters such as particle volume concentration and particle size distribution are changed. We have chosen to use as our measured quantities the Kubelka–Munk scattering and absorption parameters derived from the diffuse reflectance and transmittance spectra. In this way we can make contact with the large, but predominantly empirical, knowledge base in the coatings industry, where the Kubelka–Munk analysis is frequently used. However, these quantities are used simply as a means of parametrizing the data, and we do not assume that this simple model accurately describes the physical situation.

## II. REVIEW OF SCATTERING THEORY

### A. Mie theory

The exact analytical solution of Maxwell's equations for the scattering of an electromagnetic wave from a single sphere (Mie theory) was first presented by Gustav Mie in 1908.<sup>12</sup> It has since been described in great mathematical detail in the literature<sup>13</sup> and will not be further explicated here. Given an isotropic, spherical particle of arbitrary radius and optical constants, illuminated by electromagnetic radiation of arbitrary wavelength, Mie theory allows one to calculate the far-field extinction cross section  $C_{\text{ext}}$ , where extinction is the removal of light from the incident beam by absorption and scattering. Absorption is the transformation of the incident electromagnetic radiation into excitation within the particle, and scattering is the redirection of the incident radiation into a different propagation direction. These two contributions to extinction can be separately calculated to obtain the absorption and scattering cross sections  $C_{\text{abs}}$  and  $C_{\text{sca}}$ , with  $C_{\text{ext}} = C_{\text{abs}} + C_{\text{sca}}$ . For a nonabsorbing particle (one with a purely real index of refraction),  $C_{\text{abs}} = 0$  and  $C_{\text{sca}} = C_{\text{ext}}$ . Of particular interest in this work are the volume-normalized scattering and absorption coefficients  $S$  and  $K$ , which characterize the scattering per unit volume of the particle:

$$S = \frac{C_{\text{sca}}}{\left(\frac{\pi a^3}{6}\right)}, \quad K = \frac{C_{\text{abs}}}{\left(\frac{\pi a^3}{6}\right)}, \quad (1)$$

where  $a$  is the diameter of the particle.

In addition to these angle-independent quantities, Mie theory also allows one to calculate the angular distribution of

the scattered light. The amount of light scattered into a unit solid angle about a given direction is the differential scattering cross section  $dC_{\text{sca}}/d\Omega$ , and the angular distribution is usually expressed in terms of the angular distribution function  $G(\cos \theta)$  [most commonly called the phase function  $p(\cos \theta)$  in the light scattering literature], where  $\theta$  is the angle between the incident and scattered light:

$$G(\cos \theta) = \frac{1}{k^2 C_{\text{sca}}} \frac{dC_{\text{sca}}}{d\Omega}, \quad (2)$$

where  $k$  is the wave number  $k = 2\pi/\lambda$ , with  $\lambda$  the wavelength of light in the medium. This quantity is normalized so that its integral over all space is unity. Also of interest is the mean free path  $\xi$  for scattering and absorption by independent particles. This can be calculated from the scattering and absorption cross-sections and the number density of particles  $\rho$  using  $\xi^{-1} = \rho(C_{\text{sca}} + C_{\text{abs}}) = \eta + \chi$ .

The Mie calculations assume a spherical particle. The fact that pigment particles are not perfect spheres has been shown by finite-element calculations of scattering from particles of realistic shapes<sup>14</sup> to cause variations in the scattering parameter and angular distribution of the scattered light of the order of 6% or less in  $S$ .

### B. Kubelka–Munk

A very wide variety of multiple-scattering models and techniques have been developed over the long history of the field, particularly in astrophysical and atmospheric contexts. These methods have been reviewed and tabulated in the comprehensive work by van de Hulst.<sup>15</sup> That author in 1980 began with a single-particle scattering function (often in simplified form) and developed a multiple-scattering result to compare with observations. Throughout that work, and that of virtually every author in the field, the particles are assumed to be in one another's far field, i.e., their radiation fields are assumed to be independent, thereby permitting the addition of field intensities rather than amplitudes. While this assumption is usually valid in atmospheric research, it is not fulfilled in concentrated particulate dispersions such as paints and coatings. One multiple scattering model, the Kubelka–Munk or “two-stream” model, is a simple approach to radiation transfer in the presence of multiple scattering that is widely used in the pigment and paper industries. The model has been described extensively in the literature,<sup>9</sup> and only the salient features will be mentioned here. A homogeneous slab of thickness  $d$  (with lateral dimensions that are effectively infinite) is divided into slices of infinitesimal thickness  $dx$ , cut parallel to the slab surface, which are characterized by identical absorption and scattering parameters  $K^*$  and  $S^*$ . (The reader should note that this is not the usual notation for these quantities, but is here adopted to distinguish them from similar quantities produced by the theoretical calculations.) These empirical coefficients are not necessarily related in any direct way to the optical properties of the materials that make up the slab. Diffuse, monochromatic light is incident on the slab in the  $-x$  direction (normal to the slab). The radiation flux within each slice is divided into a forward flux  $i$  (in the  $-x$  direction) and a backward flux  $j$  (in the  $x$  direc-

tion). The scattering within the slice is assumed to be angularly isotropic, so that these two fluxes represent an average over the propagation angles  $\theta$  (with the  $-x$  direction)  $0 < \theta < 90^\circ$  and  $90 < \theta < 180^\circ$ . Solution of the appropriate coupled differential equations for the two fluxes produces the diffuse reflectance and transmittance coefficients, i.e., the fraction of incident light diffusely reflected or transmitted:

$$R = \frac{(1 - \beta^2) \sinh \kappa d}{(1 + \beta^2) \sinh \kappa d + 2\beta \cosh \kappa d}, \quad (3)$$

$$T = \frac{2\beta}{(1 + \beta^2) \sinh \kappa d + 2\beta \cosh \kappa d}, \quad (4)$$

where

$$\beta = \sqrt{\frac{K^*}{K^* + 2S^*}} \quad \kappa = \sqrt{(K^* + 2S^*)}.$$

The Kubelka–Munk model is valued more for its simplicity and ease of use than for its faithful representation of the actual experimental conditions. The derivation of Eqs. (3) and (4) assumes that the light incident upon the slab, as well as the light in every slice within the slab, is totally diffuse (i.e., has no angular dependence). The more realistic case of a collimated light source is addressed by the so-called extended Kubelka–Munk models.<sup>16</sup>

The Kubelka–Munk model also assumes diffuse radiation within each slice, which for collimated illumination will not be the case, at least in the upper slices of the slab. Some models therefore incorporate more than two radiation fluxes, and allow the scattering and absorption parameters  $S^*$  and  $K^*$  to vary with depth. Early three-flux models, such as that of Ryde<sup>17</sup> included a collimated component in the forward flux. More elaborate four-stream<sup>10,18</sup> and many-stream<sup>18,19</sup> models have been developed, as well as models that take into account variations in scattering with depth.<sup>20</sup> For large optical depths and low absorption, the photon diffusion theory<sup>11,21,22</sup> has proved useful.

All of these models can be useful within their ranges of validity. However, these ranges often do not encompass the actual experimental conditions, such as high absorption and high volume fraction occupied by particles (particle volume concentration). Also, the parameters of the models may be difficult to relate to the actual optical characteristics and concentration of the particles and medium that make up the films.

Our approach in this work is to work within the simplest of the models (the Kubelka–Munk model) and to use it as a means of parametrizing our experimental data. That is, we will extract values of  $K^*$  and  $S^*$  from the diffuse reflectance and transmittance data, and see how these parameters vary among different films. In so doing, we provide a way to relate the measured scattering properties of these realistic films to the detailed physical characteristics of the component materials and microstructures. In contrast to the standard development of radiation transfer analysis, in which the optical properties resulting from a particular set of assumptions about the single scattering characteristics and the appropriate multiple scattering model are calculated and compared with experiment,<sup>15</sup> we will begin from the single-

scattering properties of the particles and the measured optical properties and extract a multiple scattering function, using the Kubelka–Munk formalism as a parametrization method. To be useful, this approach requires only that the parameters we extract vary in a systematic way with variations in the fundamental physical characteristics of the films. The established knowledge base of Kubelka–Munk analyses of real films gives confidence that this is the case. This approach has the advantage that it does not require the very limiting assumption of independent scattering. This makes it particularly useful for real films.

### III. CALCULATION TECHNIQUES

The scattering and absorption cross sections for a single 500-nm-diam quinacridone sphere embedded in acrylic resin were calculated in the Mie theory using the BHMIE computer code by Bohren and Huffman.<sup>13</sup> Calculations were carried out for wavelengths in the range 250–850 nm at 10 nm intervals using the appropriate values for the optical constants of the particle and the medium. Because Mie theory involves an extrapolation to the infinite far field, the medium is assumed to be nonabsorbing. In the present case this is an excellent approximation for wavelengths longer than 300 nm. The optical constants of the quinacridone as a function of wavelength were kindly provided by Dr. P. Bujard of Ciba Specialty Chemicals. The optical constants of the acrylic resin were obtained from spectroscopic ellipsometry measurements performed by M. F. Lemon of DuPont. The relative refractive index (index contrast)  $m = n_{\text{particle}}/n_{\text{medium}}$  ranges from approximately 1.3 to 1.8 over this wavelength range. The Mie size parameter  $x = 2\pi a n_{\text{medium}}/\lambda$ , where  $a$  is the diameter of the sphere, ranges from 19.9 to 5.4. The particles are therefore not small compared to the wavelength (in which case Rayleigh theory would apply), or are they large enough to be in the regime of geometrical optics. In order to examine the angular distribution of the scattering, calculations of the angular distribution function  $G$  [Eq. (2)] were also made using the MIETAB program.<sup>23</sup>

## IV. EXPERIMENT

### A. Samples and measurements

The samples were prepared by D. E. Spahr of DuPont Automotive Products (Philadelphia, PA). The base resin was an acrylic resin, including dispersant, crosslinker, and solvent. The particles were quinacridone ( $C_{29}H_{12}N_2O_2$ ), Cinquasia Magenta RT-143-D from Ciba Specialty Chemicals. The as-received pigment particles were mixed in the liquid resin, and the resulting dispersion was ground for 30–60 min in a media mill. The slurry was then drawn by hand into a continuous film, using a 38  $\mu\text{m}$  (1.5 mil) blade. The film was baked at 121 °C (250 °F) for 30 min to evaporate the solvent. The substrates used were 0.090-in.-thick Viosil fused quartz plates from DuPont Photomask (Round Rock, TX), manufactured by Shin-Etsu Chemical Co. The films were dried under ambient conditions and the final thicknesses ranged from 10.3 to 15.3  $\mu\text{m}$ . The particle volume concentrations (PVCs) of the final films were 0% (for the pure resin film used as a

reference), 4.7%, 8.4%, and 13.8%. The total transmission (direct+diffuse) at 650 nm was in the range 56%–79%, depending on the PVC.

Measurements of total and diffuse reflectance and transmittance were made of the films using a Labsphere model RSA-PE-19 reflectance spectroscopy accessory (integrating sphere) attached to a Perkin-Elmer Lambda 19 UV/VIS/NIR spectrophotometer. The instrument is a dual-beam one, and uses a halogen lamp for illumination at wavelengths longer than 319 nm and a deuterium lamp at shorter wavelengths. Data were acquired over the wavelength range 250–850 nm, and were referenced to a normalized background. The scan rate was 60 nm/min, and data were taken at 1 nm intervals. The nominal bandpass was 2 nm, corresponding to an actual spectral bandwidth ranging from 2.02 nm at short wavelengths to 1.69 nm at long wavelengths. For transmittance measurements the light was normally incident on the back side of the quartz substrate, so that it passed through the substrate before encountering the film, and a quartz blank without film was placed in the reference beam. For reflectance measurements the light was incident directly on the film at an angle of 8° to the film normal. Light which exited the substrate on the back side entered a light trap and was not reflected back into the film. All measurements were made under ambient conditions.

For measurements of diffuse reflectance and transmittance, the specularly reflected or directly transmitted light was removed from the signal by placing a light trap at the appropriate position on the integrating sphere. In the transmittance measurements the trap removed the light from a cone of half-angle  $\sim 4.2^\circ$  around the directly transmitted beam, and in the reflectance measurements the cone removed had half-angle  $\sim 7.0^\circ$  around the specularly reflected beam.

### B. Data analysis

In order to extract scattering and absorption parameters from the measured diffuse reflectance and transmittance, a parametrization based on the Kubelka–Munk or two-stream model was used. The measured spectra were fitted at each wavelength to Eqs. (3) and (4) with the Kubelka–Munk parameters  $K^*$  and  $S^*$  as the fitting parameters. The fitting was performed using the GRAMS/32 software from Galactic Industries Corp., together with the programs K-MUNK, GFIT, and GFIT-S provided by Deconvolution and Entropy Consulting.<sup>24</sup> The KMUNK program uses simplex optimization to search for the scattering and extinction coefficients  $S^*$  and  $K^*$ , fitting the Kubelka–Munk equations [Eqs. (3) and (4)] to measured diffuse reflectance and diffuse transmittance spectra. The downhill simplex method of Nelder and Mead<sup>25</sup> was modified to compute  $S^*$  and  $K^*$  as wavelength-dependent vectors, and to restart with new vertices after the first convergence to mitigate the effects of collinearity.

The parameters  $K^*$  and  $S^*$  obtained from the data were then related to the absorption and scattering coefficients  $K$  and  $S$  obtained from the theoretical calculations through an interpretation suggested by Brinkworth<sup>26</sup> and Mudgett and Richards.<sup>18</sup> This interpretation results from a comparison of the two-stream Kubelka–Munk model and a more accurate

many-stream model. Mudgett and Richards found that the Kubelka–Munk absorption parameter  $K^*$  correlated well with the cross section for absorption per unit volume  $K$  according to

$$K^* = 2K. \tag{5}$$

From the same analysis, the Kubelka–Munk scattering parameter  $S^*$  is related to the cross section for scattering per unit volume of the particle  $S$  by means of the angular distribution of the scattering. There are two contributions to this angular distribution. The first is the anisotropy of the scattering from a single particle, which is obtained from the Mie theory. The normalized scattering angular distribution function  $G(\cos \theta)$  can be expanded in Legendre polynomials:

$$G(\cos \theta) = \sum_{n=0}^{\infty} a_n P_n(\cos \theta), \tag{6}$$

where  $P_n(\cos \theta)$  is the Legendre polynomial of order  $n$ . The coefficients  $a_n$  depend upon the size parameter  $x$  (and thus on the wavelength).

The second contribution to the angular distribution arises from multiple scattering, i.e., from the varying angles of incidence of the light on each particle in the film, resulting from scattering in previous layers of the film. The direction of incidence, which is perpendicular to the film surface in the upper layers of the film (since the scattering is strongly forward-peaked), will become more random as light is multiply scattered in passing through many layers. The result of this depth dependence is difficult to model in detail, but can be approached by the use of a function  $F(\cos \theta)$  which is also expanded in Legendre polynomials:

$$F(\cos \theta) = \sum_{m=0}^{\infty} b_m P_m(\cos \theta). \tag{7}$$

This function is intended to encompass the effects of multiple scattering that arise from the film microstructure, i.e., the location of the individual scatterers within the film, their interaction with one another, the volume concentration of the scatterers, and the thickness of the film. The Kubelka–Munk scattering coefficient  $S^*$  can then be expressed as the convolution of these two angular functions:

$$S^* = S \int_{-1}^1 F(\cos \theta) G(\cos \theta) d(\cos \theta). \tag{8}$$

From the properties of Legendre polynomials it can then be shown that

$$S^* = S \sum_{l=0}^{\infty} \frac{2a_l b_l}{2l+1}. \tag{9}$$

The coefficients  $a_l$  can be obtained using the Mie theory for the phase function, by fitting the angular distribution derived from a program such as MIETAB<sup>23</sup> to a sum of Legendre polynomials. To do this we have used the program GFIT, which expands  $G(\cos \theta)$  in Legendre polynomials of order 0 to  $L$ . The output is a set of  $L+1$  wavelength-dependent expansion coefficients  $\{a_0(\lambda), \dots, a_L(\lambda)\}$ , where  $L$ , the highest order of the expansion, is chosen by the user. For the range of size parameters considered here, the scattering is sharply

forward-peaked and coefficients up to  $L=22$  are needed to represent the angular distribution accurately, especially at shorter wavelengths. We then used the program GFIT\_S to fit the Kubelka–Munk scattering coefficient  $S^*$  as expressed in Eq. (9) to the Mie single-particle scattering coefficient  $S$  and the Legendre coefficients  $\{a_0(\lambda), \dots, a_L(\lambda)\}$  output from GFIT. The calculated  $\{b_0, \dots, b_L\}$  coefficients are assumed to be independent of wavelength.

The normalization of the angular distribution given in Eq. (2) requires that  $a_0 = 1/4\pi$ . Mudgett and Richards<sup>18</sup> noted that for a variety of phase functions in which forward and backward scattering were of equal intensity, a good fit to the two-stream calculation could be obtained using only one additional term  $a_1$ , with  $b_0 = -b_1 = 3/8$ . This leads to

$$S^* = \frac{3}{4} \left( a_0 - \frac{a_1}{3} \right) S. \tag{10}$$

However, in the case considered here, the phase function is dominated by forward scattering and we should not expect the same result. The correspondence between the two-stream (Kubelka–Munk) and many-stream models, from which Eq. 10 is obtained, was excellent in the cases considered by Mudgett and Richards for which the ratio of the absorption cross section to the scattering cross section,  $K/S$ , was  $10^{-3}$  or less. This same relationship between the scattering coefficients  $S^*$  and  $S$  can be derived from the photon diffusion model,<sup>11,26</sup> which also assumes that  $K/S$  is small. However, in the case considered here,  $K/S$  is not small, being between 0.05 and 1.25 for wavelengths shorter than 650 nm. In cases where  $K/S$  equaled or exceeded  $10^{-2}$ , Mudgett and Richards found that the two-stream model underestimated the transmittance by several percent or more compared to the many-stream model. We have taken the approach of fitting Eq. (9) to our data to obtain the values of  $b_l$  which best describe the real measurements and the film microstructure, and then examining the behavior of  $F(\cos \theta)$  and the coefficients as a function of particle concentration and grinding time.

## V. RESULTS

### A. Mie theory

The Mie theory calculations for  $S$  and  $K$  (the scattering and absorption cross sections per unit volume of particle) are shown in Fig. 1. These are calculated for a single, isolated particle, and are determined by the optical characteristics of the quinacridone and the acrylic resin. The quinacridone extinction coefficient has two pronounced peaks ( $k_{\text{particle}} \sim 0.8$ ) at  $\sim 300$  nm and at  $\sim 550$  nm, the latter being a double peak. The extinction coefficient has a minimum at 400 nm, and is negligible for  $\lambda > 600$  nm. The index contrast  $m$  for quinacridone in resin rises sharply as  $\lambda$  increases from 250 to 300 nm, and then declines to its original level as  $\lambda$  increases to 500 nm. There is another peak in  $m$  at 575 nm, and then another gradual decline at higher wavelengths.

The first feature to be noticed in the Mie calculations that result from these optical constants is a pronounced peak in  $S$ , and corresponding dip in  $K$ , at approximately 400 nm. This is precisely the region in which the absorption in bulk quinacridone is at a minimum, and the extinction is domi-

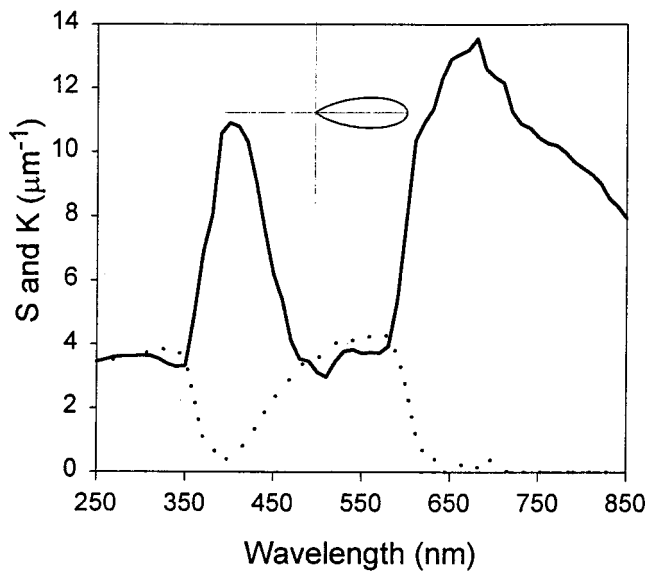


FIG. 1. Scattering coefficient  $S$  (solid line) and absorption coefficient  $K$  (dotted line) for a 500-nm-diam quinacridone sphere calculated using Mie theory. The inset shows a polar plot of the angular distribution of the scattering for  $\lambda = 500$  nm.

nated by scattering. There is a second peak in  $S$  at about 700 nm, a region in which the absorption of bulk quinacridone is again very small. At longer wavelengths  $K$  remains negligible and  $S$  falls off steadily. The index contrast  $m$  declines steadily in this region. In the region of the second peak in the quinacridone absorption,  $475 \text{ nm} < \lambda < 600 \text{ nm}$ ,  $S$  and  $K$  are approximately equal and both contribute to the extinction. This is also true in the region below 350 nm, but here the assumption that the matrix is nonabsorbing is less valid.

The angular distributions of the scattering at various wavelengths are all strongly peaked in the forward direction, as is expected for size parameters in this range (see the inset to Fig. 1). Even for the most angularly isotropic scattering, at the longest wavelength, only 7.4% of the scattered light is directed into the backwards hemisphere, and for shorter wavelengths the fraction is even lower. The average cosine of the scattering angle is in the range  $0.60 < \langle \cos \theta \rangle < 0.91$  for all wavelengths. The presence of absorption has a significant effect on the angular distribution of the scattering, causing it to be less strongly peaked in the forward direction than it would be in the absence of absorption.

## B. Experiment

Figure 2 shows the measured diffuse reflectance and transmittance as a function of wavelength (in vacuum) for the three films of different PVC. The regions of very low reflectance and transmittance between 500 and 600 nm and below 350 nm correspond to the wavelength regions of strong absorption in the quinacridone particle. The pure resin without quinacridone particles, which was also measured, is essentially transparent (except at the shortest wavelengths) and shows negligible diffuse reflectance and transmittance.

The values of  $K^*$  and  $S^*$  displayed in Fig. 3 bear some resemblance to the coefficients derived from Mie theory, but

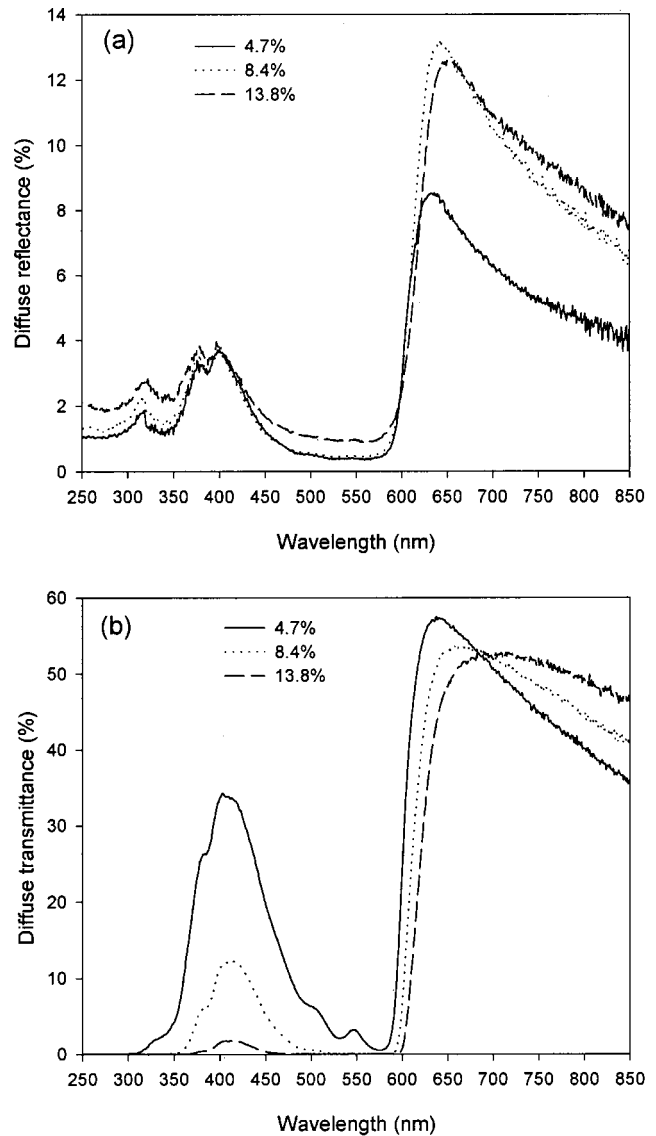


FIG. 2. Measured diffuse reflectance and transmittance for films of PVC = 4.7% (solid line), 8.5% (dotted line), and 13.8% (dashed line). (a) Diffuse reflectance. (b) Diffuse transmittance.

there are significant differences. This is to be expected since they are not defined in the same way.

In the short-wavelength region where the extinction coefficients of the quinacridone and the medium rise sharply (the quinacridone extinction coefficient being two orders of magnitude larger than that of the resin), the transmittance data for the different samples [Fig. 2(b)] show essentially zero diffuse transmittance. The calculations of  $K^*$  and  $S^*$ , which require nonzero  $T$ , are unreliable in this region and the values are not shown. Similarly, for the highest PVC, there is a zero-transmittance region in the range  $480 \text{ nm} < \lambda < 590 \text{ nm}$ . From Eq. (4) it can be seen that both  $R$  and  $T$  small corresponds to  $K^*$  large and  $K^*/S^* \gg 1$ . In this case  $T$  approaches zero as  $T \approx \exp(-K^*d)$ , and  $R$  as  $R \approx S^*/2K^*$ , independent of the film thickness  $d$ . In this wavelength region  $S^*$  increases with PVC, as does the reflectance. Thus the diffuse reflectance and transmittance in this region are

dominated by absorption, though the scattering has a minor effect on  $R$ .

Throughout the measurement range, the diffuse reflectance and transmittance are dominated by absorption rather than scattering.  $K^*$  follows the quinacridone absorption closely, but even at wavelengths where the absorption coefficient is at its minimum, the ratio  $K^*/S^*$  is larger than 2 and at some wavelengths is as high as 150. The scattering parameter  $S^*$  tends to decline where the index contrast  $m$  does, due to the reduction in the efficiency of the scattering.

In the wavelength region  $\lambda > 600$  nm, in which scattering is relatively important ( $K^*/S^* \geq 2$ ),  $S^*$  has a maximum immediately above 600 nm and declines thereafter. It is of particular interest to note that the values of  $S^*$  derived from  $R$  and  $T$  for the PVC=8.4% and the 13.8% samples are essentially identical in this wavelength range. The saturation of  $S^*$  with PVC is a particularly interesting effect. In a film of sufficiently low concentration, in which single scattering predominates, the absorption and scattering parameters would be expected to be proportional to the concentration of the particles. In that case  $K^*/S^*$  would be independent of concentration. In these films, this is true only in the wavelength regions around 400 and 625 nm where  $K^*/S^*$  has local minima. For 500 nm particles, the average distance  $L$  between particle surfaces is 885 nm for a PVC of 4.7%, 642 nm for 8.4%, and 468 nm for 13.8%. The wavelength of light in the medium ranges from 157 to 584 nm in the measured range, so the average surface-to-surface spacing is at most a few wavelengths even for the lowest concentration and smallest wavelength. In the range  $\lambda > 600$  nm, the surface-to-surface spacing is two wavelengths or less. At this distance, the interactions between the radiation fields of adjacent particles become important. Garg *et al.*<sup>22</sup> and Thiele and French<sup>14</sup> have observed correlation effects when the interparticle spacing becomes comparable to  $\lambda$ , leading to an increase in transmission as PVC is increased in concentrated dispersions. Similar effects were observed by Killey and Meeten,<sup>27</sup> in which the imaginary part of the refractive index of the dispersion reached a maximum as a function of volume concentration of particles and then decreased as the PVC was increased further. This was explained as resulting from the effect of neighboring particles on the scattering of a particular particle. Ishimaru *et al.*<sup>21</sup> observed a similar effect, in which the measured total scattering cross section decreased as the particle density increased. The diffuse reflectance curves for the PVC=8.4% and 13.8% samples are almost identical at long wavelengths, and all three diffuse transmittance curves cross at approximately 700 nm. However, even at short wavelengths, where the surface-to-surface spacing ranges from three to more than five wavelengths in the medium,  $K^*/S^*$  is not independent of concentration. Thus even at these larger spacings, the particles cannot be considered single scatterers and multiple scattering effects must be considered.

## VI. DISCUSSION

Figure 4 shows the Kubelka–Munk parameter  $K^*$  calculated from the diffuse reflectance and transmittance spectra

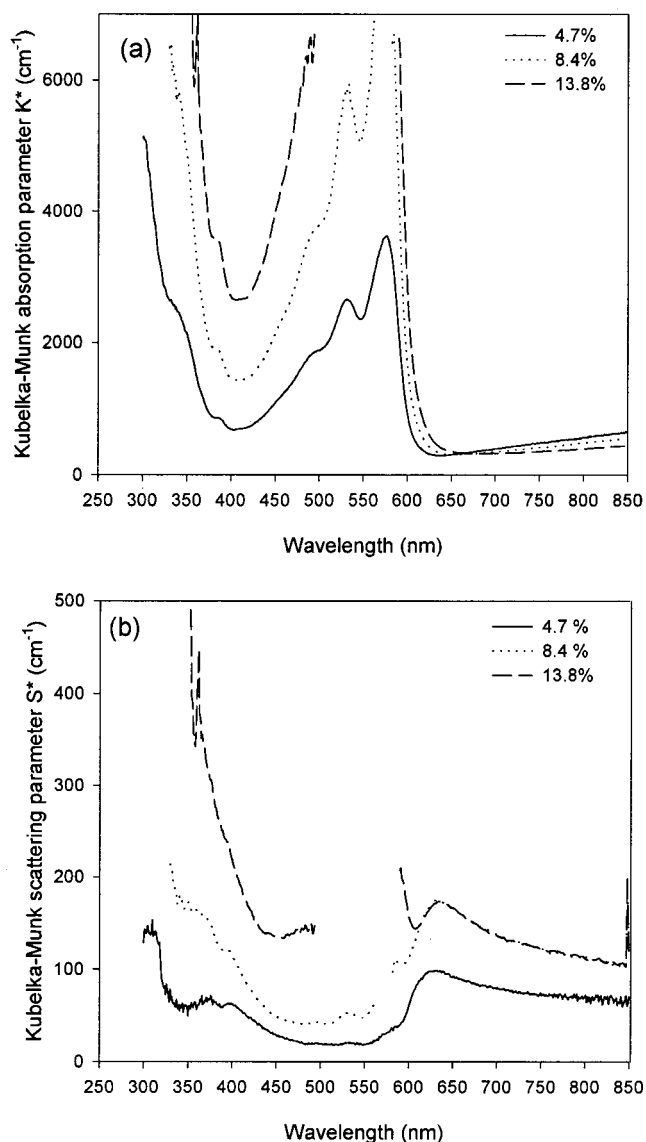


FIG. 3. Kubelka–Munk absorption parameter  $K^*$  and scattering parameter  $S^*$  for films of PVC=4.7% (solid line), 8.5% (dotted line), and 13.8% (dashed line). The gaps in the data result from saturation. (a) Absorption parameter  $K^*$ . (b) Scattering parameter  $S^*$ .

shown in Fig. 2.  $K^*$  has been divided by two for comparison with the Mie calculation, as described previously. Also shown in the figure is the Mie calculation from Fig. 1, scaled by the PVC of the film. The agreement between the two is rather remarkable considering the deficiencies of the Kubelka–Munk model in describing the actual experimental conditions. In particular, it is worth noting that in the Kubelka–Munk model,  $K^*=2K$  is to be expected if the flux in the scattering medium is perfectly diffuse. Given the strongly forward-peaked scattering from isolated particles in this regime, and the fact that the transmission is not entirely diffuse, it is perhaps rather surprising that the relationship holds as well as it does. This gives confidence that the parameterization of our data that we have chosen is correlated with the physical realities of the films. It is clear that the dominant influence on both curves is the absorption spectrum of the bulk quinacridone.

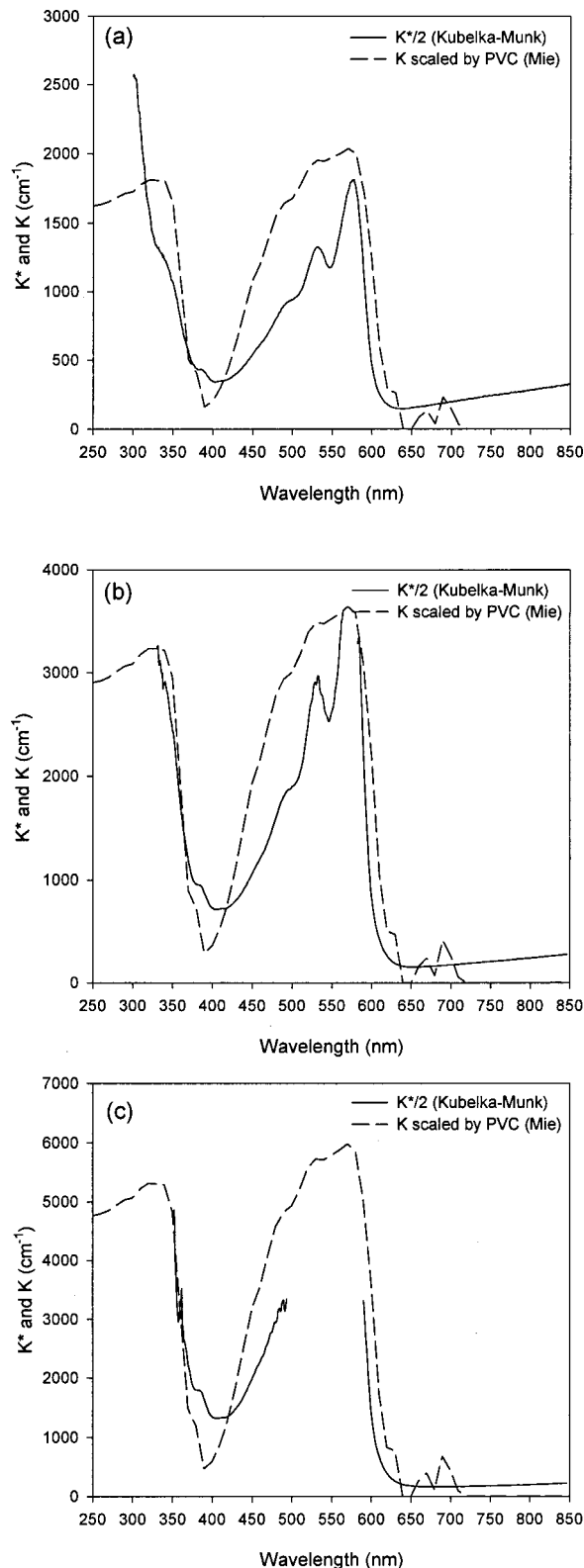


FIG. 4. Kubelka-Munk absorption parameter  $K^*/2$  (solid line) and Mie absorption coefficient  $K$  (dashed line) scaled by the PVC. The gaps in the data result from saturation. (a) PVC=4.7%. (b) PVC=8.5%. (c) PVC=13.8%.

In an effort to gain further insight into the role of single- and multiple-particle scattering phenomena, a “reflectance” was calculated in the Mie model. This was accomplished by first calculating the angular distribution function  $G(\cos \theta)$  at

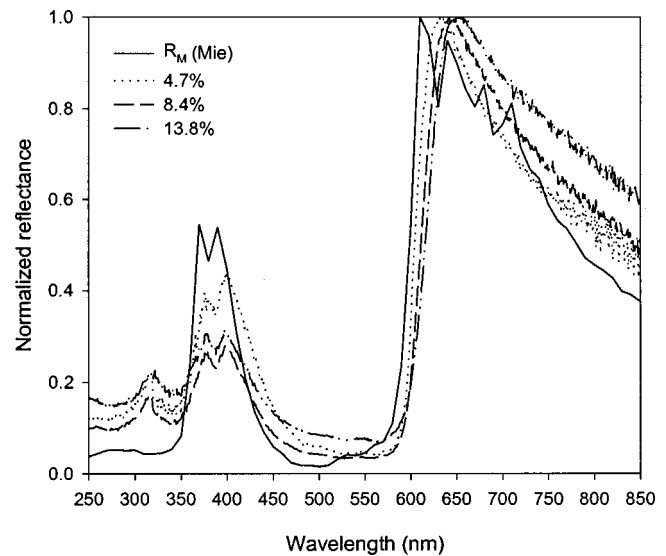


FIG. 5. “Mie reflectance”  $R_M$  calculated from Eq. (11) (solid line) compared to measured diffuse reflectance of films of PVC=4.7% (dotted line), 8.5% (dashed line), and 13.8% (dot-dash line). All curves are normalized to their maximum value.

each wavelength and integrating it over the backward hemisphere ( $-1 < \cos \theta < 0$ ). This quantity was then divided by the integral of  $G(\cos \theta)$  over all space, multiplied by the scattering efficiency  $C_{sca}/\pi(a/2)^2$  (where  $a$  is the particle diameter) to account for the variation of the total scattering with wavelength. This was in turn multiplied by the albedo  $C_{sca}/C_{ext}$  to account for absorption. The resulting “Mie reflectance”  $R_M$  is thus

$$R_M = \frac{\int_0^{-1} G(\cos \theta) d(\cos \theta)}{\int_{-1}^1 G(\cos \theta) d(\cos \theta)} \frac{C_{sca}}{\pi(a/2)^2} \frac{C_{sca}}{C_{ext}}. \quad (11)$$

The variations with wavelength of the three factors are roughly similar in shape. Figure 5 shows  $R_M$  and the measured diffuse reflectances, all normalized to their maximum values for purposes of comparison. The resemblance is striking, and emphasizes that for the films considered, the dominant factor in the variation of the reflectance with wavelength is the single-scattering characteristics of the pigment particle. The influence of multiple scattering can be seen in the variation with PVC. The diffuse reflectance for the lowest PVC is the most similar to  $R_M$ , both in the relative heights of the two peaks (at 400 and 650 nm) and in the rate of decrease of the reflectance with wavelength above 650 nm. As PVC is increased, the scattering at large wavelengths is disproportionately enhanced: the 650 peak becomes comparatively more prominent, and the decline in reflectance at large wavelengths becomes more gradual. With increasing PVC, multiple scattering becomes more important in determining the diffuse reflectance and transmittance.

Also of interest is the mean free path  $\xi$  and the optical thickness of the film  $\tau$  for independent scatterers. For the lowest PVC (4.7%),  $\xi$  is in the range  $1.5 \mu\text{m} < \xi < 3.2 \mu\text{m}$ , with the largest values of  $\xi$  occurring at wavelengths for which the absorption is small. This value is larger than the average surface-to-surface spacing  $L$  of the particles at this concentration,  $L = 0.9 \mu\text{m}$ . The transport mean free path,

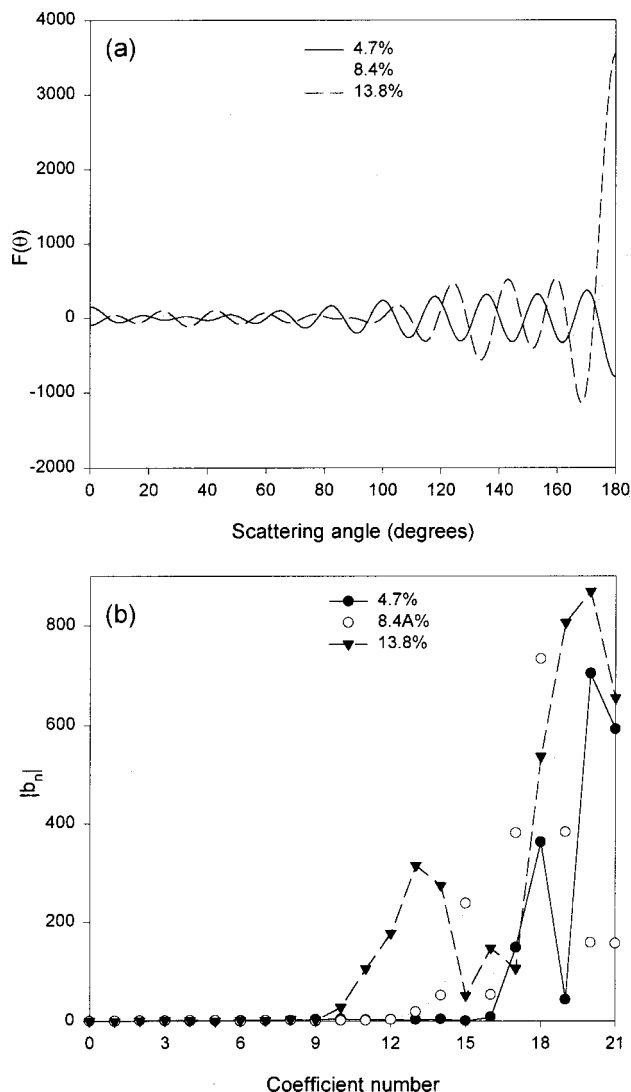


FIG. 6. Multiple scattering function  $F(\theta)$  and absolute value of Legendre coefficients  $|b_n|$  (see the text) for films of PVC=4.7% (solid line), 8.5% (dotted line), and 13.8% (dashed line). (a)  $F(\theta)$ . (b)  $|b_n|$ .

conventionally defined as  $\xi_{\text{trans}} = \xi / (1 - \langle \cos \theta \rangle)$  (where  $\langle \cos \theta \rangle$  is the average value of the scattering angle) is smaller than the film thickness for all but the shortest wavelengths. For the 4.7% film,  $\xi_{\text{trans}}$  is less than the film thickness for all wavelengths larger than 300 nm. As the PVC is increased and multiple scattering increases, the mean free path decreases. For the 8.4% film,  $0.8 \mu\text{m} < \xi < 1.8 \mu\text{m}$  and  $L = 0.6 \mu\text{m}$ , and for 13.8%  $0.5 \mu\text{m} < \xi < 1.1 \mu\text{m}$  and  $L = 0.5 \mu\text{m}$ . At this PVC  $\xi_{\text{trans}}$  is less than the film thickness at all wavelengths. Thus for the larger concentration of particles, the average interparticle spacing becomes comparable to the mean free path, and it is reasonable to expect that the assumption of independent scatters will become invalid. At the same time, the transport mean free path remains smaller than the thickness of the film.

The result of the deconvolution of  $S^*/S$  is shown in Fig. 6. Figure 6(a) shows the multiple-scattering function  $F(\theta)$  vs  $\theta$ . Although in principle  $F(\theta)$  will be different for different wavelengths [like  $G(\theta)$ ], experimentally we are limited to a single “average”  $F(\theta)$  by the fact that at each wavelength

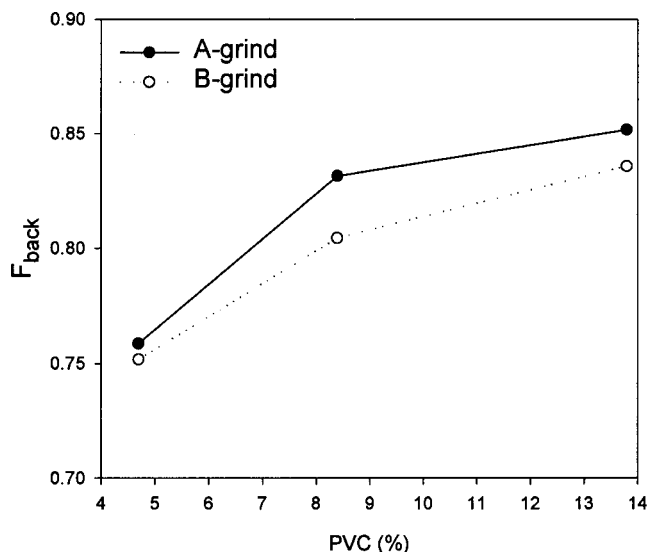


FIG. 7. Multiple-scattering backscattering fraction  $F_{\text{back}}$  (see the text) vs PVC for two different grinding times. The grinding time for the B grind (dotted line) was longer than for the A grind (solid line).

we have only one value of  $S^*/S$ . Since there is an infinite number of sets of  $b_l$  which satisfy Eq. (9) at any one wavelength, it was necessary to constrain the  $b_l$  to be the same at all wavelengths. This mathematical restriction is not an unreasonable approximation from the physical point of view, as the arrangement of the particles in the film is of course the same for all wavelengths. As is to be expected of a function built from a finite number of Legendre polynomials,  $F(\theta)$  is oscillatory in character. Note that a physically reasonable  $F(\theta)$  need not be positive at every point [unlike  $G(\theta)$ , which represents an irradiance]. While  $S^*$  is necessarily positive definite, the definition in Eq. (8) does not require that  $F(\theta)$  be so as long as its convolution with  $G(\theta)$  is. Similarly, the  $b_l$  need not be positive. What is striking about  $F(\theta)$ , as seen in Fig. 6(a), is the fact that it is strongly peaked at  $\theta = 180^\circ$ , i.e., backward scattering. This is exactly what would be expected from a function embodying the effects of multiple scattering, since it is that contribution which takes the strongly forward-peaked scattering from the individual particles and directs it into the backward hemisphere, to emerge as diffusely reflected light. Further, the predominance of the peak at  $180^\circ$  increases as the PVC increases. The more numerous the particles are, the more effective the film is at diffusing the incident collimated light.

These characteristics of  $F(\theta)$  can be seen in a different way by examining Fig. 6(b). Here the absolute values of the Legendre coefficients  $b_l$  are shown for the three PVCs. In order to produce a function  $F(\theta)$  that has sharp variation in angle, i.e., one that is strongly peaked at a particular angle ( $180^\circ$  in this case), significant contributions from Legendre polynomials of high order (large  $l$ ) are required. Thus the magnitude of the higher-order coefficients is larger than that of the lower-order ones, especially for larger PVC. Figure 6(b) also demonstrates that Mudgett and Richards’s<sup>18</sup> approximation incorporating only the first two Legendre coefficients is not adequate for cases in which  $G(\theta)$  is highly anisotropic.

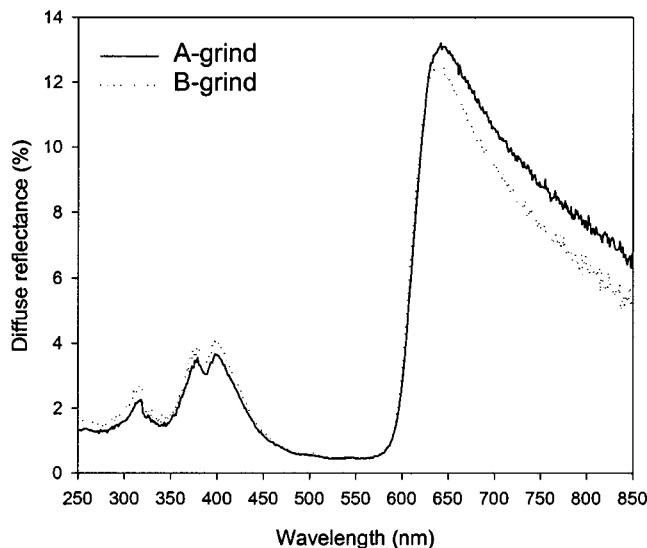


FIG. 8. Measured diffuse reflectance for two films with PVC=8.5% and two different grinding times. The grinding time for the B grind was longer than for the A grind.

The predominance of backward scattering in  $F(\theta)$ , and its dependence on PVC, can also be seen by examining the total contribution to the backward scattering. In a spirit similar to Eq. (11), this can be done by integrating the deviation of  $F(\theta)$  from zero, i.e., its absolute value, over the angular range  $90^\circ < \theta \leq 180^\circ$ :

$$F_{\text{back}} = \frac{\int_{-1}^0 |F(\cos \theta)| d(\cos \theta)}{\int_{-1}^1 |F(\cos \theta)| d(\cos \theta)}. \quad (12)$$

Since the multiple scattering function is responsible for redirecting the strongly forward-scattered light into the backward hemisphere,  $F_{\text{back}}$  would be expected to be larger than 0.5 for a film with significant diffuse reflectance, and to increase with PVC. This is indeed the case, as can be seen in Fig. 7.

It is clear from the preceding that this form of analysis, in which the single-particle and multiple-particle contributions to the Kubelka–Munk scattering parameter  $S^*$  are considered separately, is successful at giving results which are amenable to physical interpretation. To see if these interpretations can be extended beyond the particular samples with which they were developed, we now consider a set of related films. These films were prepared in the same fashion and with the same PVCs as the set analyzed previously, but with an extended grinding time. The grinding of the particle+resin slurry serves primarily to de-agglomerate clusters of particles that occur due to van der Waals interactions, rather than to reduce the size of the individual particles that make up the agglomerates. The diffuse reflectance and transmission spectra of these films were similar to those of the first set, with the most noticeable differences being a slight increase in  $R$  with extended grinding time in the 350–450 nm range, and a more significant decrease in  $R$  in the  $\lambda > 620$  nm range. The diffuse reflectance spectra for the 8.4% PVC films are compared in Fig. 8. When these films are subjected to the same analysis as the first set, using the same functions  $G(\theta)$ , the results are quite similar, as would be expected. However, there are small changes in the amplitude of the oscillations in

$F(\theta)$ , especially at angles above  $90^\circ$  (i.e., in the backscattering range). These changes result in a decrease in  $F_{\text{back}}$  at each PVC with increased grinding time, as shown in Fig. 7. The trend with PVC remains the same, however.

In order to understand this change with grinding time, we first recall that the comparison of the measured reflectance with the “Mie reflectance”  $R_M$  showed that the effects due to multiple scattering were most pronounced in the wavelength regions near 400 nm and above 650 nm where the spectra are not dominated by absorption. If the primary effect of the increased grinding time were to decrease the most common particle size, we would expect to see a shift of the sharp edge near 600 nm toward lower wavelengths, which is not observed. As seen in Fig. 5, this feature is attributable to single-particle effects, in particular to the sharp decrease in the extinction coefficient of the quinacridone. A decrease in the particle size from 500 to 400 nm would shift this feature down in wavelength by 25 nm, which is not observed. The primary effect of extended grinding time must therefore be on the particle size distribution, i.e., the “tail,” and not on the dominant particle size. Typical pigment particle distributions contain an extended “coarse tail” of particles of much larger size than the average, and extended grinding breaks up the large particles and increases the number of the average (or near average) size particles as well as the number of smaller particles (“fines”). If, for example, the grinding were to break up a 1- $\mu\text{m}$ -diam particle into eight 500 nm particles (conserving particle volume), the fractional decrease in the number  $N_{\text{large}}$  of large particles would be larger than the fractional increase in the number  $N_{\text{ave}}$  of average-size particles as long as  $N_{\text{ave}} > 8N_{\text{large}}$ , which is typical for such a distribution. The increase in  $N_{\text{ave}}$  would be expected to increase the multiple scattering, much as would an increase in the film thickness. However, the measured reflectance shows that this effect is counterbalanced by the effect of the reduction in the number of larger particles. Mie calculations show that the maximum in the scattering per unit volume ( $S$ ) of quinacridone for 550 nm light occurs for a particle diameter of 230 nm, and  $S$  declines from this maximum more steeply at smaller diameters than at larger ones. Thus under these conditions, breaking up a large particle into smaller ones, and thereby moving the particle from superoptimal to suboptimal size, reduces the total scattering even though the number of particles is increased. For example, breaking a 1  $\mu\text{m}$  particle into particles of diameter 84 nm or smaller while maintaining the same particle volume would decrease the total scattering, due to the much smaller  $S$  of the smaller particles. Particles closer to the average size would not need to be reduced to such small diameters in order to reduce the scattering: The scattering of 550 nm light from a 750 nm particle would be reduced if it were broken up into particles of diameter smaller than 95 nm. Thus the reduction in the multiple scattering produced by extended grinding can be explained as the result of a reduction in the diameter of the larger particles to below optimal size.

## VII. CONCLUSIONS

In this work we have developed a method that begins to bridge the gap between the fundamental physics of the scat-

tering of light from individual particles and the practical characterization of a film using the simple Kubelka–Munk analysis. Because the angular distribution of scattering from a single spherical particle is easily calculated using Mie theory if the real and imaginary parts of the refractive index are known, this analysis begins to make it possible to predict how changes in the optical properties, size, or concentration of the particles, or in the optical properties of the matrix, will affect the diffuse reflectance and transmission of the film. For more complicated scatters which are beyond the scope of Mie theory, such as nonspherical particles or agglomerates, this method can be used if techniques for calculating the angular distribution of the scattering from a single scatterer are available. This can be done, for example, by direct application of Maxwell's equations using finite element methods.<sup>14</sup>

### ACKNOWLEDGMENTS

We thank Dr. D. E. Spahr for preparing the samples, and for helpful discussions. We thank A. R. Hanuska for assistance with the BHMIE code, and Dr. A. Miller for assistance with the MIETAB code. We also thank M. F. Lemon for measurements of the optical constants of the base resin, Dr. P. Bujard for providing the optical constants of quinacridone, and D. J. Jones for assistance with the reflectance and transmittance measurements.

<sup>1</sup>C. F. Bohren, *Am. J. Phys.* **55**, 524 (1987).

<sup>2</sup>S. Chandrasekhar, *Radiative Transfer* (Dover, New York, 1960).

<sup>3</sup>H. M. Liao and T. W. Coyle, *J. Can. Ceram. Soc.* **65**, 254 (1996).

<sup>4</sup>S. Johnsen and E. A. Widder, *J. Theor. Biol.* **199**, 181 (1999).

<sup>5</sup>G. B. Benedek, *Appl. Opt.* **10**, 459 (1971).

<sup>6</sup>R. Barchini, J. G. Gordon II, and M. W. Hart, *Jpn. J. Appl. Phys., Part 1* **37**, 6662 (1998).

<sup>7</sup>D. G. Phillips and F. W. Billmeyer, Jr., *J. Coat. Technol.* **48**, 30 (1976).

<sup>8</sup>R. W. Johnson, E. S. Theile, and R. H. French, *Tappi J.* **80**, 233 (1997).

<sup>9</sup>P. Kubelka and F. Munk, *Z. Tech. Phys. (Leipzig)* **12**, 593 (1931); P. Kubelka, *J. Opt. Soc. Am.* **38**, 448 (1948); Gustav Kortüm, *Reflectance Spectroscopy*, translated by J. E. Lohr (Springer, New York, 1969).

<sup>10</sup>B. Maheu, J. N. Letoulouzan, and G. Gouesbet, *Appl. Opt.* **23**, 3353 (1984).

<sup>11</sup>L. F. Gate, *J. Phys. D* **4**, 1049 (1971); *Appl. Opt.* **13**, 236 (1974).

<sup>12</sup>G. Mie, *Ann. Phys. (Leipzig)* **25**, 377 (1908).

<sup>13</sup>C. F. Bohren and D. R. Huffman, *Absorption and Scattering of Light by Small Particles* (Wiley, New York, 1983); H. C. van de Hulst, *Light Scattering by Small Particles* (Wiley, New York, 1957).

<sup>14</sup>E. S. Thiele and R. H. French, *J. Am. Chem. Soc.* **81**, 469 (1998).

<sup>15</sup>H. C. van de Hulst, *Multiple Light Scattering: Tables, Formulas, and Applications* (Academic, New York, 1980).

<sup>16</sup>J. L. Sanderson, *J. Opt. Soc. Am.* **32**, 727 (1942); W. E. Vargas and G. A. Niklasson, *Appl. Opt.* **36**, 5580 (1997).

<sup>17</sup>J. W. Ryde, *Proc. R. Soc. London, Ser. A* **131**, 451 (1931).

<sup>18</sup>P. S. Mudgett and L. W. Richards, *Appl. Opt.* **10**, 1485 (1971).

<sup>19</sup>P. Latimer and S. J. Noh, *Appl. Opt.* **26**, 514 (1987).

<sup>20</sup>W. E. Vargas and G. A. Niklasson, *Appl. Opt.* **36**, 3735 (1997); *J. Opt. Soc. Am. A* **14**, 2243 (1997); **14**, 2253 (1997).

<sup>21</sup>A. Ishimaru, Y. Kuga, R. L.-T. Cheung, and K. Shimizu, *J. Opt. Soc. Am.* **73**, 131 (1983).

<sup>22</sup>R. Garg, R. K. Prud'homme, I. A. Aksay, F. Liu, and R. R. Alfano, *J. Opt. Soc. Am. A* **15**, 932 (1998); *J. Mater. Res.* **13**, 3463 (1998).

<sup>23</sup>The MIETAB program was obtained from A. Miller (electronic mail: amiller@nmsu.edu).

<sup>24</sup>Deconvolution and Entropy Consulting, 755 Snyder Hill Rd., Ithaca, NY 14850, electronic mail: www.deconvolution.com

<sup>25</sup>J. A. Nelder and R. Mead, *Comput. J. (UK)* **7**, 308 (1965).

<sup>26</sup>B. J. Brinkworth, *Appl. Opt.* **11**, 1434 (1972).

<sup>27</sup>A. Killey and G. H. Meeten, *J. Chem. Soc., Faraday Trans. 2* **77**, 587 (1981).